Operational Research in Engineering Sciences: Theory and Applications
Vol. 6, Issue 3, 2023, pp. 124-137
ISSN: 2620-1607
eISSN: 2620-1747
DOI: https://doi.org/10.31181/oresta/060306

PERFORMANCE ENHANCEMENT OF THE SURFACE ELECTROMYOGRAPHY SIGNAL USING HYBRID FEATURES SELECTION WITH AN APPLICATION ON MOVING ROBOTIC MANIPULATOR

Sadiq J. Abou-loukh[1], Ibraheem Kasim Ibraheem[2*]

[1] Department of electrical engineering, College of Engineering, University of Baghdad, Baghdad 10001, Iraq.
[2] Department of Computer Engineering Techniques, Al-Mustaqbal University College, 51001 Hilla, Iraq.

Received: 20 April 2023
Accepted: 26 September 2023
First Online: 07 October 2023

Research Paper

***Abstract**: The objective of this paper is to find a hybrid feature set that obtains good descriptive information on surface Electromyography signals to move a 4-DoF robotic hand. The hybrid feature set is obtained from the investigation of the performance of the Time Dependent Power Spectrum Descriptors(TD-PSD) feature set which consists of ($log(m_0)$, $log(m_0 - m_4)$, $log(m_0 - m_2)$, $log(S)$, $log(Irregularity\ Factor)$, $log(Waveform\ Length\ Ratio)$, and TD feature set. The proposed system was tested on datasets extracted from six healthy subjects and the results showed that the support vector machines achieved higher system accuracy with 95.61 % but with a high processing time of 2.48 sec compared to Linear Discriminant Analysis with an accuracy of 93.29% and low time processing of 0.573sec and 93.81% accuracy was achieved by K-Nearest Neighbor (K-NN)with a processing time of 1.332sec for hybrid feature set which consists of Mean Absolute Value, Root Mean Square, log(m0), and Waveform Length.*

***Keywords**: Myo Gesture Armband, Electromyography Signal, Robotic Arm, Feature Extraction, DUE Arduino, Pattern Recognition.*

[*] Corresponding author: ibraheem.i.k@ieee.org (K. Ibraheem)
doctor_sadiq@yahoo.com (S. J. Abou-Loukh)

1. Introduction

In the last decades, large efforts accomplished to facilitate the interface between the human and the robot and make them more natural and intuitive. Many technologies were invented to control robots remotely, but one of them is of great interest since it depends on signals that are produced directly from the body. Many researchers have shown that electromyography signals (EMG) appropriate for such applications, as it gives good information about limb gestures (Hassan, Abou-Loukh, & Ibraheem, 2020). One type of robotics is the robotic arm, employed in many industry fields, such as space exploration, treatment of waste in nuclear plants, and car manufacturing. Besides, the robotic arm has played an important role in biomedical engineering with able-bodied subjects (Murillo, Moreno, & Avilés, 2016; Yoshikawa, Mikawa, & Tanaka, 2007), as well as, as a prosthetic for disable-bodied subjects, such as a robotic hand and robotic arm based on the EMG signals as in (Fukuda et al., 2003; Wang, Lao, & Zhang, 2017). The electromyography signal is an electrical signal generated by muscles' relaxation and/or contraction and is administered by the nervous system. This signal relies upon the physiological and physical qualities of tissues and is viewed as an intricate signal. Surface Electromyography (sEMG) is EMG signals gathered by putting the electrodes on the outer layer of the skin. Figure (1) illustrates eight channels of the sEMG signal gained by the Myo gesture armband that begins with a low amplitude, which changes with muscle compression movement (Gheab & Saleem, 2008; Naik, 2014).

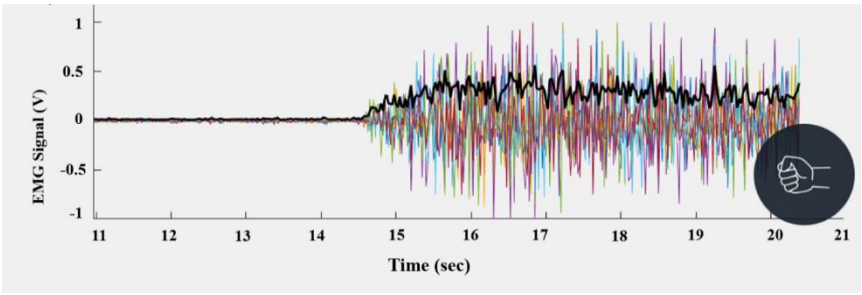

Figure 1 Raw surface electromyography (sEMG) signal acquired by the Myo gesture armband (eight channels)

There are two fundamental sorts of surface anodes that get sEMG signals, i.e., wired like a Myoware muscle sensor and wireless, for example, a Myo motion control armband. They vary in highlights, and the main contrast is the sampling rate. Data acquisition characterizes the main stage which comprises the system, that distinguishes sEMG signals, recording and prepares them by eliminating the noise and undesirable pieces of the signal, and lastly changes them to digital samples to be investigated by PC programming. Pattern recognition is the mechanized identification of patterns and consistencies in information. It addresses the foundation of sEMG signal examination and processing. To move the helping gadgets, like mechanical arms or prosthetic limbs, pattern recognition is for the most part used to get tokens of muscle action. A pattern recognition system comprises three fundamental stages, segmentation, highlight extraction determination, and characterization (Naik, Al-Timemy, & Nguyen, 2015; Ülkir, Gökmen, & Kaplanoğlu, 2017) . The sEMG signals are cut off into time slots in the segmentation stage to examine each slot alone. Two huge focuses in segmentation are the length of the section and fragment pattern; these focuses should be determined as the exactness is influenced by them (Ali, 2013). To

extract information from each window of the sEMG signals, there will be selecting suitable features in the feature extraction stage. This stage is important for the success of the system due to the chosen compatible set of features with the data analyzed and the classifier used in the system. Therefore, many researchers investigated and invented features that have good performance (Benazzouz et al., 2019; Phinyomark, N. Khushaba, & Scheme, 2018; Veer & Sharma, 2016). The features obtained from sEMG signals can be categorized by Frequency Domain (FD), Time Domain (TD), and TimeFrequency Transform (TFT). The time-dependent Power Spectrum Descriptors (TD-PSD) is a Time Domain feature set. The TD-PSD features are a set of features that have been established in 2015 by Al-Timemy et al. (2016) to minimize the processing time of the sEMG signals by extracting the spectrum moments of the power of the sEMG signal from the time domain directly. It includes six features which are, $\log(m_0)$, $log(m_0 - m_4)$, $log(m_0 - m_2)$, $log(S)$, $log(Irregularity\ Factor)$, $log(Waveform\ Length\ Ratio)$, where the m_0 , m_2 , m_4 represent the normalized of the Root Squared ZeroOrder Moment (M_0), Root Squared SecondOrder Moments (M_2), Root Squared Fourth Order Moments (M_4), respectively, while $log(S)$, log(IF), and $log(Waveform\ Length\ Ratio)$ represent Sparseness (S), Irregularity Factor (IF), and Waveform Length Ratio (WLR) (Al-Timemy et al., 2016).

In the classification stage, a suitable classifier is chosen for the system. The classifier will set the planned activity based on the previously known feature class set. The classifiers are used to recognize features of different sets. Numerous methods are adopted for classification, e.g., Linear K-Nearest Neighbor (KNN), Discriminant Analysis (LDA), Artificial Neural Network (ANN), Fuzzy Logic (FL), Support Vector Machine (SVM), Multilayer Perceptron (MLP) (Nazmi et al., 2016).

Recognition of sEMG signals is advantageous and enhances important approaches in several fields as biomedical engineering (Yang et al., 2009) and (Bitzer & Van Der Smagt, 2006), control Autonomous Flight systems (Muresan & Sadeghi Esfahlani, 2019), and also in mobile robots (Bisi et al., 2018). This paper primarily will continue the work of research (Hassan et al., 2020), by testing other features on the same data and the three well-known classifiers (SVM, LDA, and KNN) for comparison to obtain the best combination for analyzing the sEMG signals.

This paper is outlined as given next. Section 2 defines the theoretical fundamentals of the work basics of data acquisition, and pattern recognition systems. Section 3 demonstrates the proposed system to move Aideepen ROT3U robotic arm in real-time depending on sEMG signals. The experimental work and simulation results are presented in Section 4. Finally, the paper is concluded in Section 5.

2. Theoretical Background

The Myo gesture armband is a wireless wearable device and consists of eight channels, consisting of three parts: gyroscope, accelerometer, and magnetometer. Each part contains three axes x, y, and z, see Fig. 2. The Myo gesture provides two kinds of data to an application, i.e., gestural data and spatial data. The gestural data provide the user with a hand gesture and represent the data delivered for one of several predefined gestures. The spatial data which it is provides information dealing with the movement and orientation of the user's arm. The orientation represents the direction of the Myo gestures armband. It is the data acquired as a quaternion and could be

converted into the Euler angle or rotation matrix. The acceleration vector represents the Myo acceleration at any time, which is present as a three-dimensional vector (Abduo & Galster, 2015; Mannion, 2016; Murillo et al., 2016).

Figure 2 Myo gesture control armband package.

The pattern recognition algorithm presents the main methods to analyze the sEMG signals. A pattern recognition algorithm contains three main blocks, signal segmentation, feature extraction selection, and implementation of the appropriate classification to determine the class of new samples. In the pattern recognition algorithm, throughout the training stage, the input raw EMG signal is segmented, and extraction of the features is employed to convert every segment into a set of features. These features take useful data about every segment which are employed for its classification. To make the model, the pairs of hand gesture classes and features provided the algorithm of machine learning. Throughout expectation, the same extraction of the feature is employed to convert the new raw sEMG signal to feature sets. Then, these feature sets are fed into the classifier model, which creates predicted hand gesture labels (Dougherty, 2013). The scheme used in this work is an overlapping scheme for the segmentation stage. This type of segmentation split the sEMG signals into a systematic time slot that overlaps with each other. The feature extracted used in this work is the TD-PSD set of features. To extract the spectrum moments of the signal, the same technique has been used via using the derivatives and norm signals (Khushaba, Shi, & Kodagoda, 2012). The TD-PSD is a feature extraction algorithm proposed by (Al-Timemy et al., 2016). This method consists of two steps. Firstly, a set of the spectrum moments of the power of the signals is extracted directly from the time-domain depending on Parseval's theorem and the Fourier Transform (FT). This step is used to decrease the processing time spent in the time domain for feature extraction of the spectral moments of the signal. In addition, the spectrum moments of the power have been extracted logarithmically from the sEMG signals. It is essential to normalize the extracted feature to minimize the impact of noise generated due to implementing the derivatives in the first step. Secondly, the similarity of cosines is employed to evaluate the orientation between the properties of the power spectrum extracted from the raw sEMG signals, and the version of the

nonlinear cepstral. Thus, this orientation vector is used as a feature set. The TD-PSD algorithm is shown in Figure (3) (Khushaba et al., 2014).

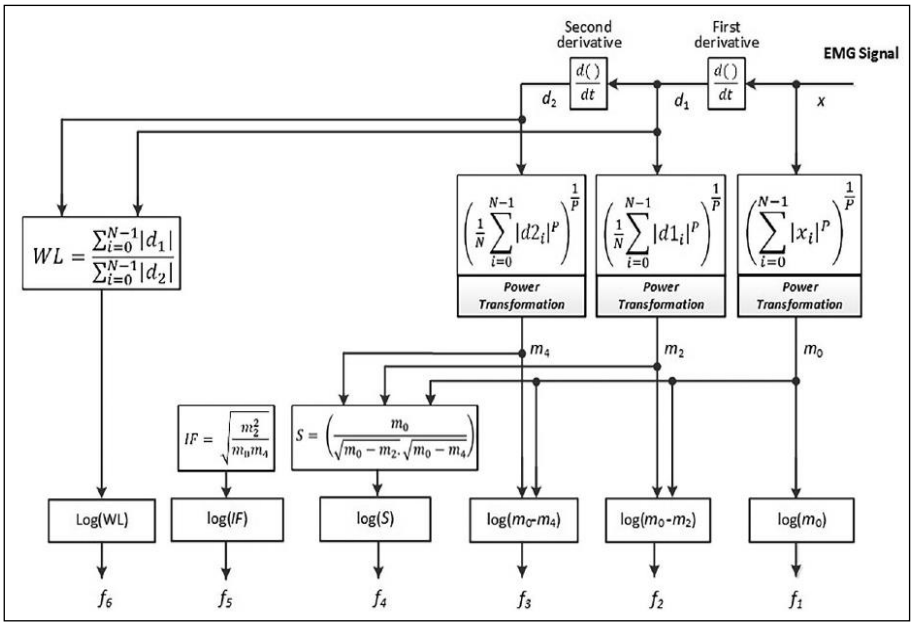

Figure 3 TD-PSD feature extraction process block diagram.

The feature extraction process starts by checking Parseval's theorem which states that the sum of the function square is equal to the sum of the transformed square (Al-Timemy et al., 2016)

$$\sum_{j=0}^{N-1} |x[j]|^2 = \frac{1}{N}\sum_{k=0}^{N-1} |X[k]X^*[k]| = \sum_{k=0}^{N-1} P[k] \quad (1)$$

As shown in Equation (1), the multiplication of $X[k]$ by its conjugate $X^*[k]$ and then the division by N produces the phase-excluded power spectrum $P[k]$, where k is the frequency index (Muresan & Sadeghi Esfahlani, 2019). Also, both the negative and positive frequencies are similar according to zero frequency in the Fourier transform (Hjorth, 1970). Therefore, because this symmetry has taken the whole spectrum, the spectral density of the power through the time domain cannot be estimated directly. So, all odd moments will be equal to zero according to the form of the frequency distribution, in agreement with the moment definition (M) of order n of the spectral density of the signal power as explained by

$$M_n = \sum_{k=0}^{N-1} k^n P[k] \quad (2)$$

Parseval's theorem is applied in (3) when n is equal to zero. Otherwise, the property of the time differentiation of the Fourier transform is applied. The *n*th differentiation of a function in the time domain named Δn for discrete-time signals is corresponding to scaling the spectrum by k raised to the *n*th power,

$$F\left[\Delta^n x[j]\right] = k^n X[k] \quad (3)$$

The informative data for each TD-PSD feature set is illustrated in Figure (3). It is represented as follows,

1. Root Squared Zero Order Moment (M_0)

This feature refers to the overall power in the frequency domain. In other words, it indicates muscle contraction strength as given in the following,

$$M_0 = \sqrt{\sum_{j=0}^{N-1} x[j]^2} \tag{4}$$

The obtained result is divided by the sum of the Zero order moment to normalize the result from all the channels.

2. Root Squared Second and Fourth-Order Moments (M_2, M_4)

The second moment represents power after the modified spectrum [□], according to Jaffar (2017).

$$M_2 = \sqrt{\sum_{k=0}^{N-1} k^2 P[k]} = \frac{1}{N}\sqrt{\sum_{k=0}^{N-1}(k\ X[k])^2} = \sqrt{\frac{1}{N}\sum_{j=0}^{N-1}(\Delta\ x[j])^2} \tag{5}$$

Fourth-Order moments can be obtained by repeating the procedure as shown below,

$$M_4 = \sqrt{\sum_{k=0}^{N-1} k^4 P[k]} = \sqrt{\frac{1}{N}\sum_{j=0}^{N-1}(\Delta^2\ x[j])^2} \tag{6}$$

Due to finding the 2nd and 4th differentiation of the signals, then the total energy is minimized. Consequently, the effect of the noise on all moments is minimized. The normalized scope of the moments (m_0 , m_2 , and m_4) is applied based on the power transformer as follows,

$$m_0 = \frac{M_0^{\lambda}}{\lambda} \tag{7}$$

$$m_2 = \frac{M_2^{\lambda}}{\lambda} \tag{8}$$

$$m_4 = \frac{M_4^{\lambda}}{\lambda} \tag{9}$$

where □=0.1. The first three features can be extracted as illustrated below:

$$f_1 = \log(m_0) \tag{10}$$

$$f_2 = \log(m_0 - m_2) \tag{11}$$

$$f_3 = \log(m_0 - m_4) \tag{12}$$

3. Sparseness

The S feature is the fourth feature that decides the energy of a vector, it is stuffed into only a few components.

$$f_4 = \log\left(\frac{m_0}{\sqrt{m_0 - m_2}\sqrt{m_0 - m_4}}\right) \tag{13}$$

4. Irregularity Factor (IF)

IF is the fifth feature which computes the ratio of the number of upward zero crossings (ZC) to that of the number of peaks. According to Subasi (2013), it represents the spectral moments of a signal. The feature can be written as

$$f_5 = \log\left(\frac{ZC}{NP}\right) = \log\left(\frac{\sqrt{\frac{m_2}{m_0}}}{\sqrt{\frac{m_4}{m_2}}}\right) = \log\left(\frac{m_2}{\sqrt{m_4 m_0}}\right) \quad (14)$$

5. Waveform Length Ratio (WLR)

This feature divides the waveform length of the 1st derivative by the waveform length of the 2nd derivative, where WLR is the summation of the absolute value of the signal derivatives. This feature can be written as:

$$f_6 = log\left(\frac{\sum_{j=0}^{N-1}|\Delta x|}{\sum_{j=0}^{N-1}|\Delta^2 x|}\right) \quad (15)$$

The feature set which consists of six features represents a model of cepstral of the sEMG effectiveness that through the raw sEMG signals can extract the characteristics of the power spectrum. In the classification stage, the same three well-known classifiers(SVM, LDA, KNN) deployed by Hassan et al. (2020) would be adopted in this work.

3. Methodology and hardware components

The primary aim of this study is to investigate the TD-PSD feature set and compare its performance with the TD one used by Hassan et al. (2020) to build a comfortable real-time system that controls a robotic arm. The wireless Myo gesture armband is the sEMG acquisition equipment used in this study. Also, the comparison between the techniques of the pattern recognition system is made to get the best-suited techniques for the best performance. The overlap technique is used to segment the sEMG data. The TD-PSD feature set is chosen to extract valuable data from each piece. Finally, three classification techniques (KNN, LDA, and SVM) to get the best performance are compared. Figure (4) shows all parts of the system.

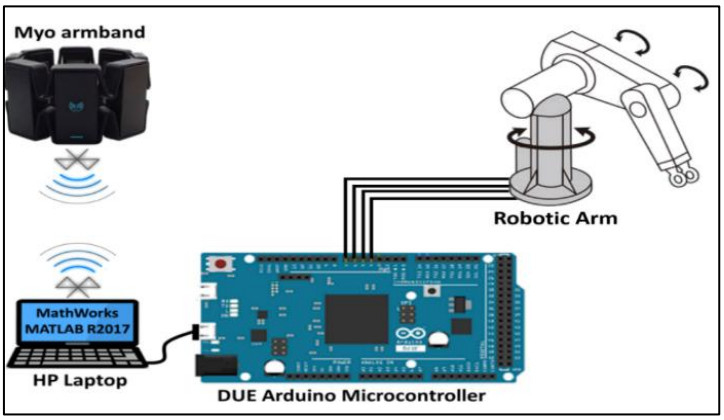

Figure 4 Overall proposed system block diagram

The Due Arduino microcontroller is used to connect the laptop to the 3-DoF Aideepen ROT3U robotic arm and send the final gesture predicted by the classifier to the robotic arm through the serial port. It has a rotation angle of 180 degrees, a height

of 42cm (holder closed), maximum opening of 4.5cm, and the most long distance of the holder is 10cm. The robotic arm consists of four brushed DC servo motors type MG 996R as shown in Figure (5).

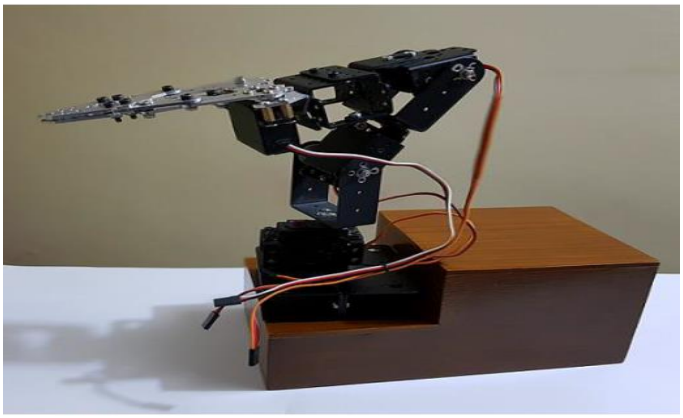

Figure 5 Aideepen ROT3U robotic arm

The same hand gestures in (Hassan et al., 2020) have been used in this study which is shown in Figure (6). The same dataset (Hassan et al., 2020) is used in this study for honest comparison. The data used in this study for six healthy subjects is given in Table (1).

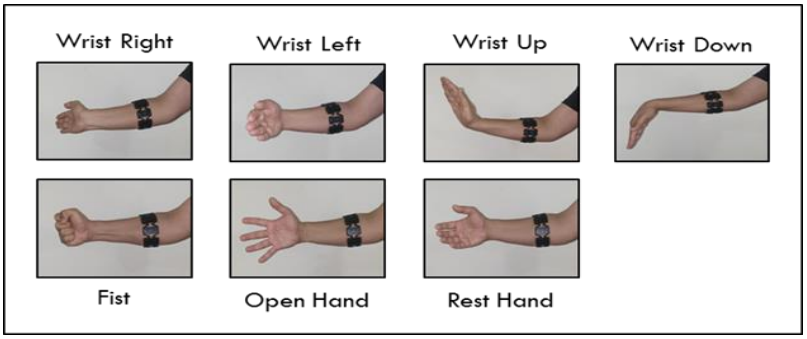

Figure 6 Hand gestures of the suggested system (Hassan et al., 2020)

Table 1. Volunteered subjects information (Hassan et al., 2020)

No. of Subject	Gender	Length (cm)	Weight (Kg)	Age (Year)	Hand side
Subject 1	Male	185	110	47	Right
Subject 2	Male	190	97	44	Right
Subject 3	Female	165	72	43	Right
Subject 4	Female	165	80	37	Right
Subject 5	Female	178	100	36	Right
Subject 6	Female	165	63	25	Right

To make the prediction model, the training model should be predefined to learn the classifier. Where the labels of hand gestures and features data of the sEMG signals are provided to the algorithm of the machine learning. To expect the gesture of new raw sEMG data, the same segmentation, and extracted features of the training model are employed and then fed into the classifier model. Figure (7) shows the pattern recognition algorithm process.

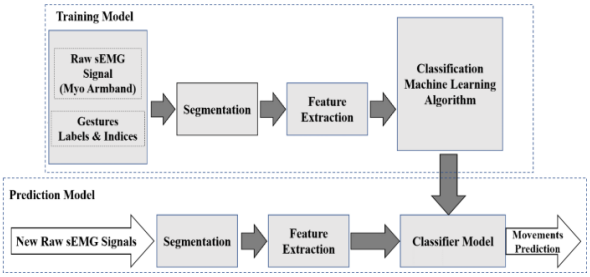

Figure 7 Pattern recognition algorithm

4. Result and Discussion

Three experiments (one for each classifier) are tested in this proposal to obtain the suitable combination for the best performance and compared with the result (Hassan et al., 2020). The TD-PSD feature set is tested for each subject, which consists of six features; log(IF), $\log(m_0)$, $log(m_0 - m_4)$, $log(m_0 - m_2)$, $log(S)$, log(WLR) .Tables 2 - 4 measure the system accuracy for each TD-PSD feature and the three classifiers (SVM, LDA, and KNN) across all subjects. Tables (2-4) show that the feature $\log(m_0)$ has good descriptive information on datasets, but the other five features in the TD-PSD set have no satisfying descriptive information for sEMG datasets. The accuracy is calculated using the following formula (Hassan et al., 2020),

$$acuracy = \frac{No.\ of\ correct\ prediction}{total\ No.of\ prediction} \times 100 \qquad (16)$$

where the number of correct predictions is the correct output from the compression of the predictions class with class testing, while the total prediction is all the expected movements from the classifier. Figure (8) shows the system accuracy result of the TD-PSD feature set with the three classifiers.

Table 2. System accuracy (%) result of each feature TD-PSD feature set with SVM classifier crosses all subjects.

No. of Subject	$\log(m_0)$	$\log(m_0 - m_2)$	$\log(m_0 - m_4)$	$log(S)$	log(IF)	log(WLR)	All features
Subject1	94.20	53.32	34.77	36.19	49.89	16.00	92.17
Subject2	88.00	56.43	33.50	34.32	51.76	20.30	89.70
Subject3	91.78	45.90	26.06	25.68	41.02	15.72	92.39
Subject4	89.90	52.74	30.47	27.58	45.78	17.33	92.91
Subject5	93.64	45.48	35.82	37.17	48.96	16.20	92.67
Subject6	91.62	53.28	28.82	28.31	37.82	16.90	90.98
Average	91.52	51.19	31.58	31.54	45.87	17.07	91.80
STD	2.31	4.46	3.77	4.93	5.45	1.69	1.23

Table 3. System accuracy (%) result of each feature TD-PSD feature set with LDA classifier crosses all subjects.

No. of Subject	$\log(m_0)$	$\log(m_0 - m_2)$	$\log(m_0 - m_4)$	$log(S)$	log(IF)	log(WLR)	All features
Subject1	88.56	51.97	24.72	34.74	49.39	17.31	89.37
Subject2	83.85	53.57	27.21	33.62	50.81	20.91	87.67
Subject3	91.28	44.78	21.93	22.81	40.21	12.38	93.83
Subject4	90.48	52.16	22.46	25.86	45.73	18.26	93.32
Subject5	92.10	45.44	29.67	34.57	47.22	16.26	93.30
Subject6	89.65	52.22	22.34	28.28	37.49	16.88	91.15
Average	89.32	50.02	24.72	29.98	45.14	17.00	91.44
STD	2.95	3.85	3.14	5.07	5.25	2.79	2.50

Table 4. System accuracy (%) result of each feature TD-PSD feature set with KNN=7 classifier crosses all subjects

No. of Subject	$\log(m_0)$	$\log(m_0 - m_2)$	$\log(m_0 - m_4)$	$log(S)$	log(IF)	log(WLR)	All features
Subject1	95.67	47.75	37.73	33.15	44.42	16.77	76.00
Subject2	87.70	51.14	38.70	31.36	44.56	17.19	69.23
Subject3	89.18	39.54	29.83	22.45	33.25	14.26	67.83
Subject4	89.35	47.01	35.88	25.48	40.76	14.90	68.58
Subject5	92.31	43.22	36.62	33.17	42.13	14.42	68.12
Subject6	93.62	46.89	32.43	28.51	32.59	17.13	70.19
Average	91.31	45.92	35.20	29.02	39.62	15.78	69.99
STD	3.06	4.02	3.40	4.37	5.39	1.39	3.06

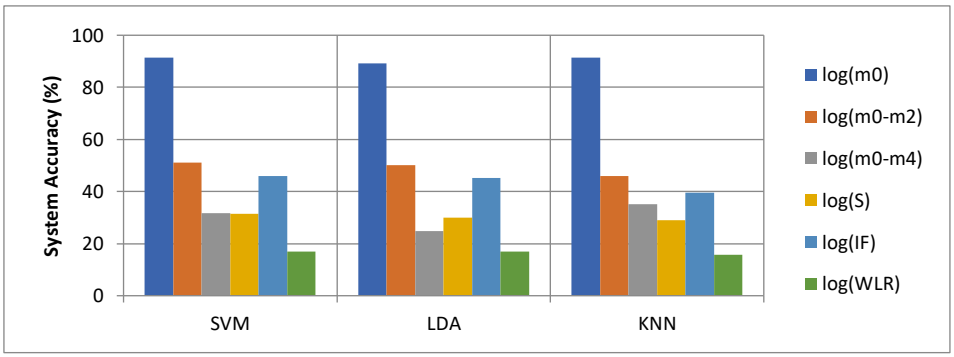

Figure 8 The average system accuracy (%) result for each feature in TD-PSD set with each classifier.

Depending on the results (Hassan et al., 2020) of testing the TD set which consists of six-time domain features (RMS, MAV, WL, AR, ZC, and SSC), it is clear that the features RMS, MAV, and WL have better performance over others. Table (4) shows that the KNN classifier (with$K = 7$) has a smaller accuracy compared with the other two classifiers, whereas such a technique is not considered in the KNN classifier. The KNN classification entirely depends on the feature space, unlike the SVM and LDA which enhance the feature space to reach a good separation between different classes. Figure (9) show the TD-PSD feature space.

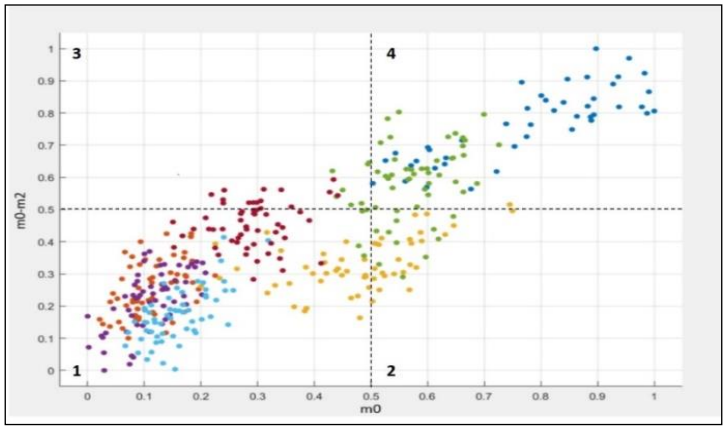

Figure 9 Scatter plot of the TD-PSD feature space

By observing the feature space in Figure (9), it appears that the interference between classes is a little complicated, especially in the first quarter, which shows the overlap between four classes. Such overlap affects the KNN predictions. In such situations reduction techniques help the KNN classifier to reduce the interference of data and improve the true predictions. The second test is a time-consuming meter. In this test, each feature would be tested and evaluated for how much time processing consumes. The processing time depends on many factors related to the hardware specification of the computer, operating system state, the number of tasks at a time, etc. However, when testing the features under approximately the same conditions has indicated how long each feature would consume time for processing. This test was applied for both feature sets (TD, and TD-PSD). Figure (10) shows the processing time for each feature. As shown, the WL feature has a smaller processing time than the log(S) feature which consumes the largest processing time. The AR feature consists of four embedded features (order four). Therefore, it is consuming a larger processing time than others on the TD feature set. In the TD-PSD feature set, all features consume a large processing time except $\log(m_0)$ which has a reasonable time. Depending on the results of all tests made in the two studies as in Hassan et al. (2020) and also in this paper, it could create a hybrid feature set that consists of (RMS, MAV, WL, and $\log(m_0)$) were chosen. The results of the hybrid features set for SVM, LDA, and KNN classifiers are shown in Table (5). Table (6) calculates the processing time for the hybrid feature set with the three classifiers SVM, LDA, and KNN. To summarize the feature selection tests, Figure (11) shows a comparison of the three feature sets used TD, TD-PSD, and hybrid features set. As a result, the hybrid feature set consists of four Time Domain features: RMS, MAV, WL, and $\log(m_0)$ with the LDA classifier were selected to be the best parameters for the system to be applied in the online mode which achieves 93.29% of system accuracy and timely processing of 0.573 seconds.

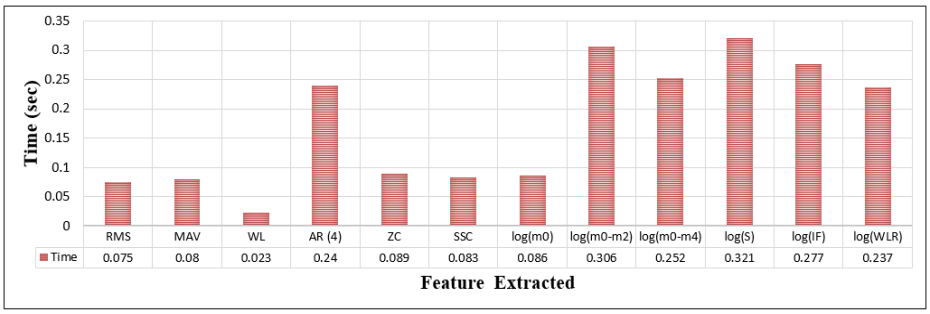

Figure 10 The time processing for each feature used in this study.

Table 5. System Accuracy (%) of hybrid feature set with all classifiers

No. of Subject	Hybrid Set + SVM	Hybrid Set + LDA	Hybrid Set + KNN
Subject1	97.79	93.90	96.41
Subject2	94.03	92.00	92.94
Subject3	95.50	94.15	93.70
Subject4	95.02	93.68	91.96
Subject5	95.93	94.32	93.79
Subject6	95.37	91.69	94.08
Average	95.61	93.29	93.81
STD	1.25	1.14	1.48

Table 6. Processing time of hybrid feature set with all classifiers

The Modules	Processing Time (sec)
Hybrid Set + SVM	2.480
Hybrid Set + LDA	0.573
Hybrid Set + KNN	1.332

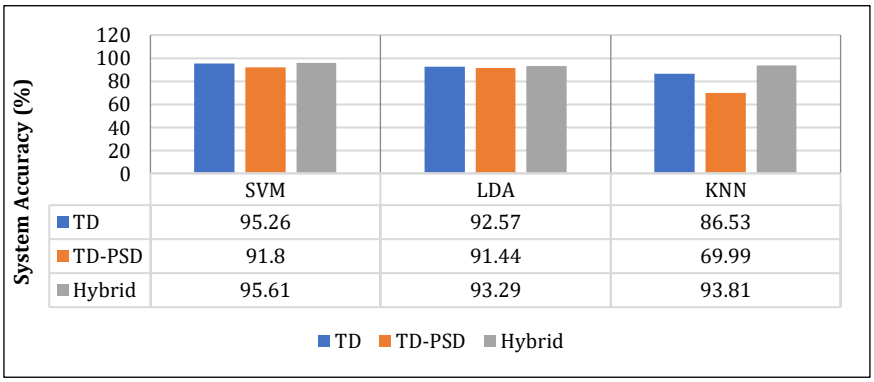

Figure 11 Comparison results of the three feature sets with all classifiers

5. Conclusion

The log (m_0) feature in the TD-PSD set is an interesting feature that led to the powerful description for such type of data set used in this work. Also, the hybrid set (RMS, MAV, WL, and log(m_0)) has higher performance than the individual TD and TD-PSD sets. Moreover, the SVM classifier has higher accuracy compared with the other two classifiers (LDA, KNN). While the LDA classifier has a low componential cost and high accuracy compared with the other two classifiers such as SVM, and KNN. For future work, a recommendation would be to demonstrate control design methods like those in Subasi (2013), Goen (2014), and Mane et al. (2015) to improve the performance of the robot arm motion.

References

Abduo, M., & Galster, M. (2015). Myo gesture control armband for medical applications. University of Canterbury. http://hdl.handle.net/10092/14449

Al-Timemy, A. H., Khushaba, R. N., Bugmann, G., & Escudero, J. (2016). Improving the performance against force variation of EMG controlled multifunctional upper-limb prostheses for transradial amputees. IEEE Transactions on Neural Systems and Rehabilitation Engineering, 24(6), 650-661. https://doi.org/10.1109/TNSRE.2015.2445634

Ali, A. H. (2013). An investigation of electromyographic (EMG) control of dextrous hand prostheses for transradial amputees. (Doctoral dissertation, University of Plymouth). http://hdl.handle.net/10026.1/2860

Benazzouz, A., Guilal, R., Amirouche, F., & Slimane, Z. E. H. (2019). EMG Feature selection for diagnosis of neuromuscular disorders. In 2019 International Conference on Networking and Advanced Systems (ICNAS) (pp. 1-5). IEEE. https://doi.org/10.1109/ICNAS.2019.8807862

Bisi, S., De Luca, L., Shrestha, B., Yang, Z., & Gandhi, V. (2018). Development of an EMG-controlled mobile robot. Robotics, 7(3), 36. https://doi.org/10.3390/robotics7030036

Bitzer, S., & Van Der Smagt, P. (2006). Learning EMG control of a robotic hand: towards active prostheses. In Proceedings 2006 IEEE International Conference on Robotics and Automation, 2006. ICRA 2006. (pp. 2819-2823). IEEE. https://doi.org/10.1109/ROBOT.2006.1642128

Dougherty, G. (2013). Pattern Recognition and Classification An Introduction. Springer New York, NY. https://doi.org/10.1007/978-1-4614-5323-9

Fukuda, O., Tsuji, T., Kaneko, M., & Otsuka, A. (2003). A human-assisting manipulator teleoperated by EMG signals and arm motions. IEEE transactions on robotics and automation, 19(2), 210-222. https://doi.org/10.1109/TRA.2003.808873

Gheab, N. H., & Saleem, S. N. (2008). Comparison study of electromyography using wavelet and neural network. Al-Khwarizmi Engineering Journal, 4(3), 108-119. https://www.iasj.net/iasj/article/2390

Goen, A. (2014). Classification of EMG signals for assessment of neuromuscular disorders. International Journal of Electronics and Electrical Engineering, 2(3), 242-248. https://doi.org/10.12720/ijeee.2.3.242-248

Hassan, H. F., Abou-Loukh, S. J., & Ibraheem, I. K. (2020). Teleoperated robotic arm movement using electromyography signal with wearable Myo armband. Journal of King Saud University-Engineering Sciences, 32(6), 378-387. https://doi.org/10.1016/j.jksues.2019.05.001

Hjorth, B. (1970). EEG analysis based on time domain properties. Electroencephalography and clinical neurophysiology, 29(3), 306-310. https://doi.org/10.1016/0013-4694(70)90143-4

Jaffar, Y. H. (2017). Design and Implementation Of A Controlled Prosthetic Hand Based On Electromyography Signal For Transradial Amputee People. (M. Sc. Thesis, University of Baghdad).

Khushaba, R. N., Shi, L., & Kodagoda, S. (2012). Time-dependent spectral features for limb position invariant myoelectric pattern recognition. In 2012 International Symposium on Communications and Information Technologies (ISCIT) (pp. 1015-1020). IEEE. https://doi.org/10.1109/ISCIT.2012.6380840

Khushaba, R. N., Takruri, M., Miro, J. V., & Kodagoda, S. (2014). Towards limb position invariant myoelectric pattern recognition using time-dependent spectral features. Neural Networks, 55, 42-58. https://doi.org/10.1016/j.neunet.2014.03.010

Mane, S., Kambli, R., Kazi, F., & Singh, N. (2015). Hand motion recognition from single channel surface EMG using wavelet & artificial neural network. Procedia Computer Science, 49, 58-65. https://doi.org/10.1016/j.procs.2015.04.227

Mannion, P. (2016). Myo armband: Wearables design focuses on packaging. EDN. https://www.edn.com/myo-armband-wearables-design-focuses-on-packaging

Muresan, B., & Sadeghi Esfahlani, S. (2019). Autonomous flight and real-time tracking of unmanned aerial vehicle. In Intelligent Computing: Proceedings of the 2018 Computing Conference, Volume 1 (pp. 945-956). Springer. https://doi.org/10.1007/978-3-030-01174-1_73

Murillo, P. U., Moreno, R. J., & Avilés, O. (2016). Individual robotic arms manipulator control employing electromyographic signals acquired by myo armbands. International Journal of Applied Engineering Research, 11(23), 11241-11249. https://www.researchgate.net/publication/314079352

Naik, G. R. (2014). Applications, Challenges, And Advancements In Electromyography Signal Processing. IGI Global. https://doi.org/10.4018/978-1-4666-6090-8
Naik, G. R., Al-Timemy, A. H., & Nguyen, H. T. (2015). Transradial amputee gesture classification using an optimal number of sEMG sensors: an approach using ICA clustering. IEEE Transactions on Neural Systems and Rehabilitation Engineering, 24(8), 837-846. https://doi.org/10.1109/TNSRE.2015.2478138
Nazmi, N., Abdul Rahman, M. A., Yamamoto, S.-I., Ahmad, S. A., Zamzuri, H., & Mazlan, S. A. (2016). A review of classification techniques of EMG signals during isotonic and isometric contractions. Sensors, 16(8), 1304. https://doi.org/10.3390/s16081304
Phinyomark, A., N. Khushaba, R., & Scheme, E. (2018). Feature extraction and selection for myoelectric control based on wearable EMG sensors. Sensors, 18(5), 1615. https://doi.org/10.3390/s18051615
Subasi, A. (2013). Classification of EMG signals using PSO optimized SVM for diagnosis of neuromuscular disorders. Computers in biology and medicine, 43(5), 576-586. https://doi.org/10.1016/j.compbiomed.2013.01.020
Ülkir, O., Gökmen, G., & Kaplanoğlu, E. (2017). Emg Signal Classification Using Fuzzy Logic. Balkan Journal of Electrical and Computer Engineering, 5(7), 97–101. https://doi.org/10.17694/bajece.337941
Veer, K., & Sharma, T. (2016). A novel feature extraction for robust EMG pattern recognition. Journal of medical engineering & technology, 40(4), 149-154. https://doi.org/10.3109/03091902.2016.1153739
Wang, N., Lao, K., & Zhang, X. (2017). Design and myoelectric control of an anthropomorphic prosthetic hand. Journal of Bionic Engineering, 14(1), 47-59. https://doi.org/10.1016/S1672-6529(16)60377-3
Yang, D.-p., Zhao, J.-d., Gu, Y.-k., Wang, X.-q., Li, N., Jiang, L., Liu, H., Huang, H., & Zhao, D.-w. (2009). An anthropomorphic robot hand developed based on underactuated mechanism and controlled by EMG signals. Journal of Bionic Engineering, 6(3), 255-263. https://doi.org/10.1016/S1672-6529(08)60119-5
Yoshikawa, M., Mikawa, M., & Tanaka, K. (2007). A myoelectric interface for robotic hand control using support vector machine. In 2007 IEEE/RSJ International Conference on Intelligent Robots and Systems (pp. 2723-2728). IEEE. https://doi.org/10.1109/IROS.2007.4399301